ADVANCES IN ATMOSPHERIC SCIENCES, VOL. 22, NO. 5, 2005, 711–719

A Model for Retrieval of Dual Linear Polarization Radar Fields from Model Simulation Outputs

LIU Liping*[1,3] (刘黎平), ZHANG Pengfei[3] (张鹏飞), Qin XU[2],
KONG Fanyou[4] (孔凡铀), and LIU Shun[3] (刘 舜)

[1] *State Key Laboratory of Severe Weather, Chinese Academy of Meteorological Sciences, Beijing* 100081

[2] *National Severe Storm Laboratory , National Oceanic and Atmospheric Administration, Norman, Oklahoma, USA*

[3] *The Cooperative Institute for Mesoscale Meteorological Studies, University of Oklahoma, Norman, Oklahoma, USA*

[4] *The Center for Analysis Prediction of Storms, University of Oklahoma, Norman, USA*

(Received 28 December 2004; revised 2 June 2005)

ABSTRACT

An algorithm for retrieving polarimetric variables from numerical model fields is developed. By using this technique, radar reflectivity at horizontal polarization, differential reflectivity, specific differential phase shift and correlation coefficients between the horizontal and vertical polarization signals at zero lag can be derived from rain, snow and hail contents of numerical model outputs. Effects of environmental temperature and the melting process on polarimetric variables are considered in the algorithm. The algorithm is applied to the Advanced Regional Prediction System (ARPS) model simulation results for a hail storm. The spatial distributions of the derived parameters are reasonable when compared with observational knowledge. This work provides a forward model for assimilation of dual linear polarization radar data into a mesoscale model.

Key words: polarimetric radar, retrieval of polarimetric variables, model output

1. Introduction

Dual-polarization radars transmit and receive horizontal and vertical polarized electromagnetic waves. Because the sizes, shapes and spatial orientations and the thermodynamic phases of hydrometeors in the atmosphere are different, their polarimetric properties are different. A polarimetric radar has the capability to distinguish different types of hydrometeors such as hail, snow, and rain, and also to estimate the amount of hydrometeors (Doviak et al., 2000). Thus, radar has been used for quantitative precipitation estimation, hydrometeor classification and discrimination between meteorological and non-meteorological scatterers (Ryzhkov and Zrnic, 1996; Brandes et al., 2001; Liu and Chandrasekar, 2000; Ryzhkov and Zrnic, 1998; Brunkow et al., 2000; Schuur et al., 2003; Zrnic and Ryzhkov, 1998). One of the important advantages of dual polarization measurements is that they can be used to assess parameters of the raindrop size distribution and to estimate precipitation more accurately (Gorgucci et al., 2002; Vivekanandan et al., 1999).

Doppler radar data have been used to analyze and to retrieve mesoscale structures of precipitation in previous works. Most of these works used radial velocity and/or reflectivity only, which includes pure kinematic and four-dimensional variational methods (Xu et al., 2001; Qiu and Xu, 1992; Sun and Crook, 1997). The initial wind, temperature, moisture and precipitation fields in the models are modified by using the Doppler radar data. The Doppler radar observations are also widely used in weather forecasting, especially nowcasting (Dixon and Wiener, 1993; Wilson and Mueller, 1993; Pierce and Hardaker, 2000). It is known that the microphysical processes play an important role in the initiation, evolution and decay of storms. Dual polarization radar has the potential to improve cloud physicsparameterizations in numerical models and to create better simulations and forecasts of severe weather.

The object of this study is to develop an algorithm to retrieve the dual polarization radar measurements

*E-mail: lpliu@cams.cma.gov.cn

from a numerical model's outputs. The cloud physics of the model and the retrieval algorithm are described in section 2. The experimental results are presented in section 3. Conclusions and discussions follow in section 4.

2. Methodology

For most mesoscale models, such as the Advanced Regional Prediction System (Xue et al., 1995), MM5 and the Coupled Ocean/Atmosphere Mesoscale Prediction System (COAMPS) (Hodur, 1997), the bulk method is used in the microphysics parameterization. Our current method is developed to obtain dual-polarimetric variables based on numerical model outputs that include five microphysical variables: water vapor, pristine ice, snow, rain and graupel. All these five microphysical variables are derived from their mixing ratios in the model (Lin et al., 1983). The size distribution of hydrometeors is assumed to be the Marshall and Palmer distribution (Marshall and Palmer, 1948). The number concentration parameters of rain, snow and graupel are set to be constants. The slope factors or drop median volume diameters vary with the mixing ratios q of the hydrometeors. The size distributions and relationship between slope factors and mixing ratios of rain, snow and graupel are

$$N(D) = N_{0(\mathrm{r,s,g})} \exp(-\lambda_{\mathrm{r,s,g}} D) \,, \tag{1}$$

$$\lambda_{\mathrm{r,s,g}} = \left(\frac{\pi \rho_{\mathrm{r,s,g}} N_{0(\mathrm{r,s,g})}}{\rho q_{\mathrm{r,s,g}}} \right) \,, \tag{2}$$

where q is the mixing rate of a given hydrometeor in kg kg^{-1}; the subscripts r, s, and g are for rain, snow, and graupel, respectively. $N_{0\mathrm{r}}$=8×10^6 m^{-4}, $N_{0\mathrm{s}}$ =4×10^6 m^{-4}, and $N_{0\mathrm{g}}$= 4×10^6 m^{-4} are number concentration parameters of rain, snow and graupel, respectively. ρ in kg m^{-3} is the density of air. ρ_{r}=10^3 kg m^{-3}, ρ_{s}=100 kg m^{-3}, ρ_{g}=200 kg m^{-3} are densities of rain, snow and graupel particles.

2.1 *Reflectivity*

The reflectivity Z (mm^6 m^{-3}) at each model grid point contains three components: rain, snow and graupel. The contributions of pristine ice and cloud droplets can be neglected because their sizes are relatively small. Thus,

$$Z = Z_{\mathrm{r}} + Z_{\mathrm{s}} + Z_{\mathrm{g}} \,, \tag{3}$$

where Z is equivalent reflectivity; and $Z_{\mathrm{r}}, Z_{\mathrm{s}}, Z_{\mathrm{g}}$ are equivalent reflectivity for rain, snow, and graupel. Based on Smith et al. (1975), each of the reflectivity components can be estimated as follows:

Rain:

$$Z_{\mathrm{r}} = \frac{10^{18} \times 720 (\rho q_{\mathrm{r}})^{1.75}}{\pi^{1.75} N_{0\mathrm{r}}^{0.75} \rho_{\mathrm{r}}^{1.75}} \,, \tag{4}$$

Dry snow:

$$Z_{\mathrm{ds}} = \frac{10^{18} \times 720 K_{\mathrm{i}}^2 \rho_{\mathrm{s}}^{0.25} (\rho q_{\mathrm{s}})^{1.75}}{\pi^{1.75} K_{\mathrm{r}}^2 N_{0\mathrm{s}}^{0.75} \rho_{\mathrm{i}}^2} \,, \tag{5}$$

Wet snow:

$$Z_{\mathrm{ws}} = \frac{10^{18} \times 720 (\rho q_{\mathrm{s}})^{1.75}}{\pi^{1.75} N_{0\mathrm{s}}^{0.75} \rho_{\mathrm{s}}^{1.75}} \,, \tag{6}$$

Dry graupel:

$$Z_{\mathrm{dg}} = \frac{10^{18} \times 720 K_{\mathrm{i}}^2 \rho_{\mathrm{g}}^{0.25} (\rho q_{\mathrm{g}})^{1.75}}{\pi^{1.75} K_{\mathrm{r}}^2 \rho_{\mathrm{i}}^2 N_{0\mathrm{g}}^{0.75}} \,, \tag{7}$$

Wet graupel:

$$Z_{\mathrm{wg}} = \left(\frac{10^{18} \times 720}{\pi^{1.75} N_{0\mathrm{g}}^{0.75} \rho_{\mathrm{g}}^{1.75}} \right)^{0.95} (\rho q_{\mathrm{g}})^{1.66} \,, \tag{8}$$

where K_{i}=0.176 is the dielectric factor for ice and K_{r}=0.93 for water; ρ is the density of air; and $\rho_{\mathrm{r}}, \rho_{\mathrm{i}}, \rho_{\mathrm{s}}$ and ρ_{g} are the densities for water, ice, snow and graupel, respectively. Note that the melting processes of snow and graupel have a great impact on the reflectivity measurements. Figure 1 shows the relation between the reflectivities of rain, dry snow and graupel and their mixing ratios. The reflectivity of rain is about 7.0 dB higher than dry snow or graupel. The reflectivities of melted snow and grapuel are also calculated. The results show that the reflectivities of wet snow and graupel are 20 dB and 12 dB higher than rain, respectively.

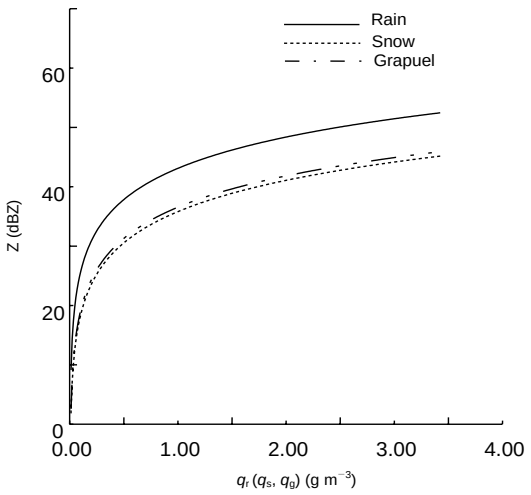

Fig. 1. Relationship between reflectivity Z and mixing ratios $q_{\mathrm{r}}, q_{\mathrm{s}}$, and q_{g}.

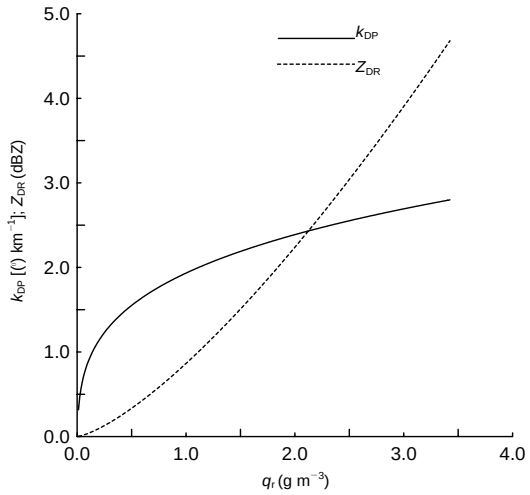

Fig. 2. Relationship between $K_{\rm DP}$ (solid line) and $Z_{\rm DR}$ (dashed line) and $q_{\rm r}$ for rain.

2.2 *Differential reflectivity*

The differential reflectivity $Z_{\rm DR}$ in dB units is defined as $10\log(Z_{\rm H}/Z_{\rm V})$. If in a radar resolution volume, the hydrometeors are mixture of rain, snow and graupel, then Z_{DR} becomes:

$$Z_{\rm DR} = 10\log\frac{Z_{\rm Hr}+Z_{\rm Hs}+Z_{\rm Hg}}{Z_{\rm Vr}+Z_{\rm Vs}+Z_{\rm Vg}}\,, \tag{9}$$

where $Z_{\rm Hr}, Z_{\rm Hs}$, and $Z_{\rm Hg}$ are reflectivity factors for rain, snow and graupel for the horizontal polarization, respectively. $Z_{\rm Vr}$, $Z_{\rm Vs}$, and $Z_{\rm Vg}$ are the reflectivity factors for the vertical polarization. For different hydrometeors in a resolution volume, $\rm Z_{H(r,s,g)}$ and $Z_{\rm DR}$ are known. Thus the reflectivity factors for the vertical polarizations $Z_{\rm V(r,s,g)}$ can be obtained,

$$Z_{\rm V(r,s,g)} = Z_{\rm H(r,s,g)} \times 10^{-0.1Z_{\rm DR(r,s,g)}}\,. \tag{10}$$

For the Marshall-Palmer drop size distribution, the differential reflectivity for rain ($Z_{\rm DRr}$) is given quantitatively by (Seliga et al., 1981)

$$Z_{\rm DRr} = \frac{53.8}{\lambda_{\rm r}} - 0.47 \quad \lambda_{\rm r} < 53.7\,{\rm cm}^{-1}\,. \tag{11}$$

Figure 2 shows the relationships between the differential reflectivity $Z_{\rm DRr}$ and the specific differential phase shift $K_{\rm DPr}$ (described in section 2.3) and their mixing ratios. $Z_{\rm DRr}$ increases sharply when $q_{\rm r}$ is less than $0.5\,{\rm g\,m^{-3}}$, yet the relationship between $K_{\rm DPr}$ and $q_{\rm r}$ is nearly linear.

For solid hydrometeors, it is difficult to find a quantitative relationship between differential reflectivity and snow or graupel contents because of the complicated shape, orientation and phase of the solid hydrometeors. In general, $Z_{\rm DR}$ for dry snow is smaller than that of rain and can be assumed to be 0.3 dB (Ryzhkov et al., 1998; Schuur et al., 2003). Larger snowflakes apparently are more likely to tumble and wobble than small crystals as they fall in the atmosphere. Thus their $Z_{\rm DR}$ is generally less than 0.2 dB. For ice crystals, their $Z_{\rm DR}$ is an order of magnitude larger than snow. A dual linear polarization radar (KOUN) has observed an averaged $Z_{\rm DR}$ of about 1.4 dB for ice crystals in the Joint Polarization Experiments (Schuur et al., 2003). The environmental temperature is a main factor affecting the shape of snowflakes. Based on the observed results, the differential reflectivity for rain and snow as a function of temperature is given by:

$$Z_{\rm DR} = \begin{cases} 0.4\,, & T \leqslant -20^{\circ}{\rm C}\,, \\ 0.2 - T \times 0.01\,, & -20^{\circ}{\rm C} \leqslant T \leqslant 0^{\circ}{\rm C}\,, \\ Z_{\rm DRr}\,, & T > 0^{\circ}{\rm C}\,, \end{cases} \tag{12}$$

where T (°C) is the environmental temperature. Snow particles are melted into raindrops when they fall into air with a temperature higher than 0°C.

Small hail particles tend to be more spherical, therefore, their $Z_{\rm DR}$ is approximately 0 dB. Large hail particles might be spherical, or they could be prolated to produce $Z_{\rm DR} < 0$ dB. Tumbling motions can make non-spherical hail of any size appear to be isotropic or spherical. So the average $Z_{\rm DR}$ is approximately 0 dB (Hubbert et al., 1998; Vivekanandan et al., 1993).

Melted graupels have a larger reflectivity and differential reflectivity than dry particles. Larger melted graupels might be more prolated to produce negative $Z_{\rm DR}$. The differential reflectivity of graupel is calculated as:

dry graupel:

$$Z_{\rm DRg} = -0.5\ {\rm dB}\,,$$

wet graupel:

$$Z_{\rm DRg} = \begin{cases} 0.0\,, & Z \leqslant 55\ {\rm dB}Z\,, \\ -0.25\,, & 55\ {\rm dB}Z \leqslant Z \leqslant 60\ {\rm dB}Z\,, \\ -0.5\,, & Z > 60\ {\rm dB}Z\,, \end{cases} \tag{13}$$

Figure 3 is the differential reflectivity contour for different $q_{\rm r}$ and dry $q_{\rm g}$. Using the figure, the contribution to the total $Z_{\rm DR}$ from rain and dry graupels can be estimated. In the area mixed with rain and dry graupels, rain dominates the contribution to the total $Z_{\rm DR}$. Dry graupels make the total $Z_{\rm DR}$ approach zero. In general, the contribution of dry graupels is small. But as they melt, the corresponding reflectivity increases greatly.

2.3 *Specific differential phase shift*

For horizontal and vertical polarization radar waves, non-spherical hydrometeors produce not only different powers of back-scattering, but also different

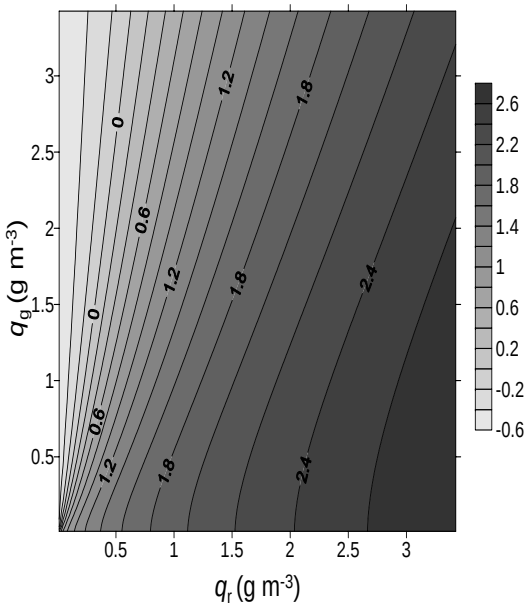

Fig. 3. Relationship between $Z_{\rm DR}$ and $q_{\rm r}$ and $q_{\rm g}$ for mixtures of rain and graupel.

propagation speeds. The former is described by $Z_{\rm DR}$ as discussed in section 2.2, and the latter is described by the specific differential phase shift $K_{\rm DP}$.

In the area mixed with rain, snow and hail, the total specific differential phase shift $K_{\rm DP}$ can be obtained by:

$$K_{\rm DP} = K_{\rm DPr} + K_{\rm DPs} + K_{\rm DPg} \,, \tag{14}$$

where $K_{\rm DPr}, K_{\rm DPs}$, and $K_{\rm DPg}$ are the $K_{\rm DP}$ for rain, snow and hail, respectively.

From the M-P drop size distribution, the relationship between rainfall rate R (mm h^{-1}), slope factor $\lambda_{\rm r}$ (mm^{-1}) and $K_{\rm DP}$ for rain are given by (Sachidananda and Zrnic, 1987; Doviak and Zrnic, 1993)

$$R = 20.35 K_{\rm DPr}^{0.866} \,, \quad \lambda_{\rm r} = 4.1 R^{-0.21} \ ({\rm mm}^{-1}) \,. \tag{15}$$

So the $K_{\rm DPr}$ [(°) km^{-1}] can be calculated from

$$K_{\rm DPr} = 72.19 \lambda_{\rm r}^{-5.49} \,. \tag{16}$$

The relationship between $K_{\rm DPr}$ and $q_{\rm r}$ is shown in Fig. 2. $K_{\rm DPr}$ reaches 5° km^{-1} when $q_{\rm r}$ equals 4 g m^{-3}.

According to the observations of a snow storm in Oklahoma (Ryzhkov et al., 1998), the average $K_{\rm DP}$ of pure snow does not follow a systematic trend with changes in the radar reflectivity factor if $Z < 35$ dBZ. The $K_{\rm DP}$ of snow increases as the height increases and the air temperature decreases. Ice crystals produce a larger specific differential phase $K_{\rm DP}$ than dry aggregated snow. The average specific differential phase of larger snowflakes is about 0.06° km^{-1} and the value for ice crystals is about 0.2° km^{-1}.

For pristine and moderately aggregated snow, the snow content is given by (Ryzhkov et al., 1998)

$$C_{\rm zw} = \frac{C K_{DP}}{1 - Z_{\rm DR}^{-1}} \,, \tag{17}$$

$$C = \frac{C_1 \lambda}{30\pi} \,, \tag{18}$$

where $C_{\rm zw}$ (g m^{-3}) is snow content, λ (cm) is radar wavelength, and C, C_1 are constants.

Because the $Z_{\rm DR}$ of snow cannot be obtained directly from model outputs, the following formula (Vivekanandan et al., 1994) is applied to calculate the $K_{\rm DPs}$ in areas of low differential reflectivity ($Z_{\rm DR}$=0.7 dB):

$$K_{\rm DPs} = 320 \rho q_{\rm s} \,. \tag{19}$$

It should be noted that for heavily aggregated snow, Eq. (17) is expected to be less reliable and it is likely to overestimate the actual ice content. This is because $K_{\rm DP}$ and $Z_{\rm DR}$ are small for large aggregates that have low density, are nearly spherical in shape, and tumble while falling.

Several factors make $K_{\rm DP}$ insensitive to graupel or hail. First, the dielectric constant is smaller for ice than for liquid. Nonetheless, for large, wet hail ($D > 20$ mm), the water coatings are thin and there may be only marginal increases in the dielectric constant. Second, hail is found in lower concentrations than other hydrometeor types. Third, the propagation through tumbling hail (statistically isotropic) should be insensitive to polarization (Straka et al., 2000). In this case, the specific differential phase shift of graupel is set to be 0.25° km^{-1}.

2.4 *Correlation coefficient at zero lag* $|\rho_{\rm HV}(0)|$

In parameters observed by dual linear polarization radar, the correlation coefficient at zero lag $|\rho_{\rm HV}(0)|$ between horizontally and vertically polarized echoes cannot be described by the model output quantitatively. $|\rho_{\rm HV}(0)|$ is affected by both the variability in the horizontal and vertical sizes of the hydrometeors and the differential phase shift. It decreases with increasing diversity of hydrometeor orientations and shapes (Zrnic et al., 1993). The components of $|\rho_{\rm HV}(0)|$ for each type of hydrometeor are examined next.

In theory, $|\rho_{\rm HV}(0)|$ for rain is generally close to unity because of the raindrop shapes and orientations. Slight departures from near unity are due to a continual change in shape, oscillations, coalescence, and breakup of the raindrops (Balakrishnan and Zrnic, 1990). $|\rho_{\rm HV}(0)|$ for rain is set to 0.97 in the current algorithm.

For snow, decorrelation can be significant when particles are wet or when they are large and irregular in shape. Moreover, $|\rho_{\rm HV}(0)|$ becomes lower in the presence of different types of hydrometeors than just one type (Jameson, 1989). Thus, $|\rho_{\rm HV}(0)|$ is set to be 0.95 for dry snow and 0.75 for wet snow in this study.

Balakrishnan and Zrnic (1990) showed that $|\rho_{\rm HV}(0)|$ decreases as (1) the hail size increases, (2) the hail protuberance-to-diameter ratio increases, (3) the hail size distributions broaden, (4) the hail is wetted or becomes spongy, or (5) the hail mixes with other hydrometeors with different distributions and sizes. For wet/spongy hail, there is a marked reduction in $|\rho_{\rm HV}(0)|$ at $D \approx 20$ mm, and a more substantial reduction in $|\rho_{\rm HV}(0)|$ at $D > 50$ mm because of resonance effects. In the current algorithm, $|\rho_{\rm HV}(0)|$ of graupel is given by:

dry graupel:

$$|\rho_{\rm HV}(0)| = 0.93\ , \tag{20}$$

wet graupel:

$$|\rho_{\rm HV}(0)| = \begin{cases} 0.91\ , & Z \leqslant 55\ {\rm dB}Z\ , \\ 0.89\ , & 55\ {\rm dB}Z \leqslant Z \leqslant 60\ {\rm dB}Z\ , \\ 0.87\ , & Z > 60\ {\rm dB}Z\ . \end{cases} \tag{21}$$

It should be noted that the above formulas are for single components of the hydrometeors. For wet snow and graupel, the melting process decreases $|\rho_{\rm HV}(0)|$. Actually, several different types of hydrometeors can coexist at the same model grid point. For example, rain, wet snow and graupel coexist at a grid point where the air temperature is below 0°C.

According to the definition of $|\rho_{\rm HV}(0)|$,

$$|\rho_{\rm HV}(0)| = \frac{\left|\sum\limits_{i=1}^{M} E^*_{\rm HH}(i) E_{\rm VV}(i)\right|}{\sqrt{S_{\rm HH} S_{\rm VV}}}\ , \tag{22}$$

where M is the number of particles, and $E_{\rm HH}(i)$ and $E_{\rm VV}(i)$ are the back scattering electric fields of the ith particle for the horizontal and vertical polarizations, respectively. $S_{\rm HH}$ and $S_{\rm VV}$ are the back-scattering energies. In the area mixed with hydrometeors, the total E and S can be divided into three components for rain, snow and graupel:

$$\begin{cases} E^*_{\rm HH}(i) = E^*_{\rm HH1}(i) + E^*_{\rm HH2}(i) + E^*_{\rm HH3}(i)\ , \\ E_{\rm VV}(i) = E_{\rm VV1}(i) + E_{\rm VV2}(i) + E_{\rm VV3}(i)\ , \\ S_{\rm HH} = S_{\rm HH1} + S_{\rm HH2} + S_{\rm HH3}\ , \\ S_{\rm VV} = S_{\rm VV1} + S_{\rm VV2} + S_{\rm VV3}\ . \end{cases} \tag{23}$$

Here, the subscripts 1, 2 and 3 are for rain, snow and graupel, respectively. The random movements of hydrometeors in the radar resolution volume cause $\sum E^*_{\rm HHi} \cdot E_{\rm VVJ=0}$ when $i \neq j$. So $|\rho_{\rm HV}(0)|$ at the grid point with a mixture of rain, snow and graupel can be rewritten as follows depending on the definitions of reflectivity and correlation coefficients,

$$\begin{aligned} |\rho_{\rm HV}(0)| = & \frac{|\rho_{\rm HV1}(0)|}{\sqrt{\left(1+\frac{Z_{\rm H2}}{Z_{\rm H1}}+\frac{Z_{\rm H3}}{Z_{\rm H1}}\right)\left(1+\frac{Z_{\rm V2}}{Z_{\rm V1}}+\frac{Z_{\rm V3}}{Z_{\rm V1}}\right)}} \\ & + \frac{|\rho_{\rm HV2}(0)|}{\sqrt{\left(1+\frac{Z_{\rm H1}}{Z_{\rm H2}}+\frac{Z_{\rm H3}}{Z_{\rm H2}}\right)\left(1+\frac{Z_{\rm V1}}{Z_{\rm V2}}+\frac{Z_{\rm V3}}{Z_{\rm V2}}\right)}} \\ & + \frac{|\rho_{\rm HV3}(0)|}{\sqrt{\left(1+\frac{Z_{\rm H1}}{Z_{\rm H3}}+\frac{Z_{\rm H2}}{Z_{\rm H3}}\right)\left(1+\frac{Z_{\rm V1}}{Z_{\rm V3}}+\frac{Z_{\rm V2}}{Z_{\rm V3}}\right)}}\ . \end{aligned} \tag{24}$$

3. Result analysis

A bow-shaped squall line case simulated (Nascimento，2002) by the ARPS (the Advanced Regional Prediction System) model is selected to examine our method. The horizontal and vertical resolutions are 2 km and 0.4 km, respectively. The numbers of grid points in the X, Y and vertical directions are 145, 181 and 48, respectively. The microphysics parameterization includes the Kessler warm rain microphysics parameterization and the three-category ice-phased (cloud ice, snow and graupel/hail) parameterization (Lin et al, 1983). The Klemp boundary layer condition is used (Klemp and Durran, 1983).

Figure 4 shows the horizontal distributions of the mixing ratios of rain and graupel at the 2-km height of the model grid partial squall line in the 5-hour simulation. At this level, most of the snow has melted into rain. Five heavy rain and graupel centers are observed in the figure. The heavy graupel centers are close to the rain centers. This implies that most of the rain is from melted graupel. Figure 5 shows the corresponding polarimetric variables derived from model outputs. The maximum reflectivity of 65 dBZ and differential reflectivity of 4.0 dB are located at the rain and graupel centers. Note that the existence of graupel increases the reflectivity and decreases the differential reflectivity. The high $Z_{\rm DR}$ (>3.5 dB) area in Fig. 5b is consistent with the rain center at X=175 km and Y=78 km in Fig. 4a. On the other hand, the graupel center located at (182 km, 82 km) corresponds to the 0 dB$Z_{\rm DR}$ area. $K_{\rm DP}$ is mainly related to the rain content, while the large $K_{\rm DP}$ ($> 5^\circ$ km^{-1}) is observed at the rain centers. In the rain region, $|\rho_{\rm HV}(0)|$ is about 0.97, and it decreases to 0.87 in the mixing region of rain and grapuel. The decrease of $|\rho_{\rm HV}(0)|$ is due to the mixture of different types of hydrometeors.

Figure 6 shows the vertical cross sections of rain,

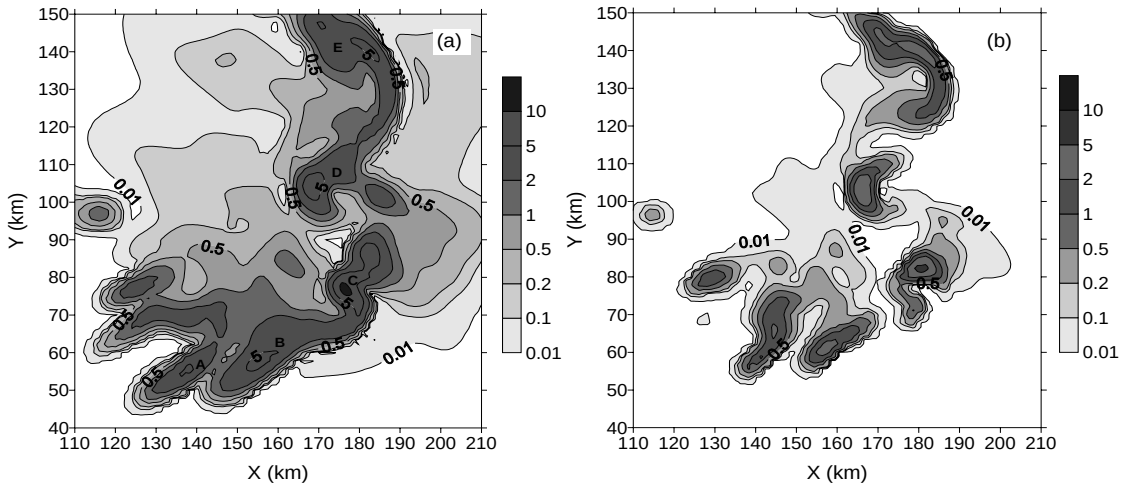

Fig. 4. Horizontal distributions of (a) q_r and (b) q_g at the 2-km height (units: 10^{-3} kg kg^{-1}). The letters A. B, C, D and E in (a) indicate the 5 heavy rain centers.

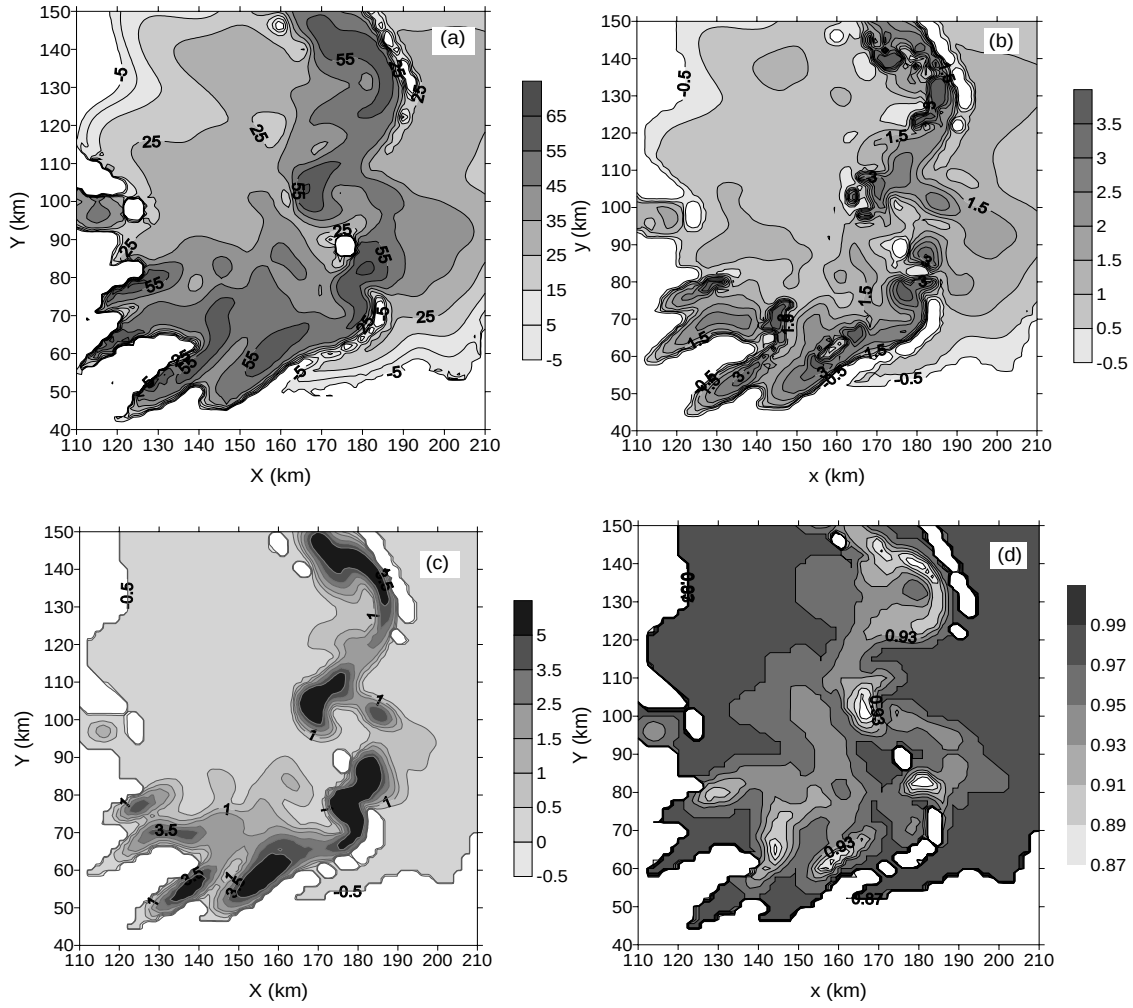

Fig. 5. Corresponding polarimetric variables retrieved from the model outputs (Fig. 4). (a) reflectivity, (b) differential reflectivity, (c) specific phase shift, and (d) correlation coefficient.

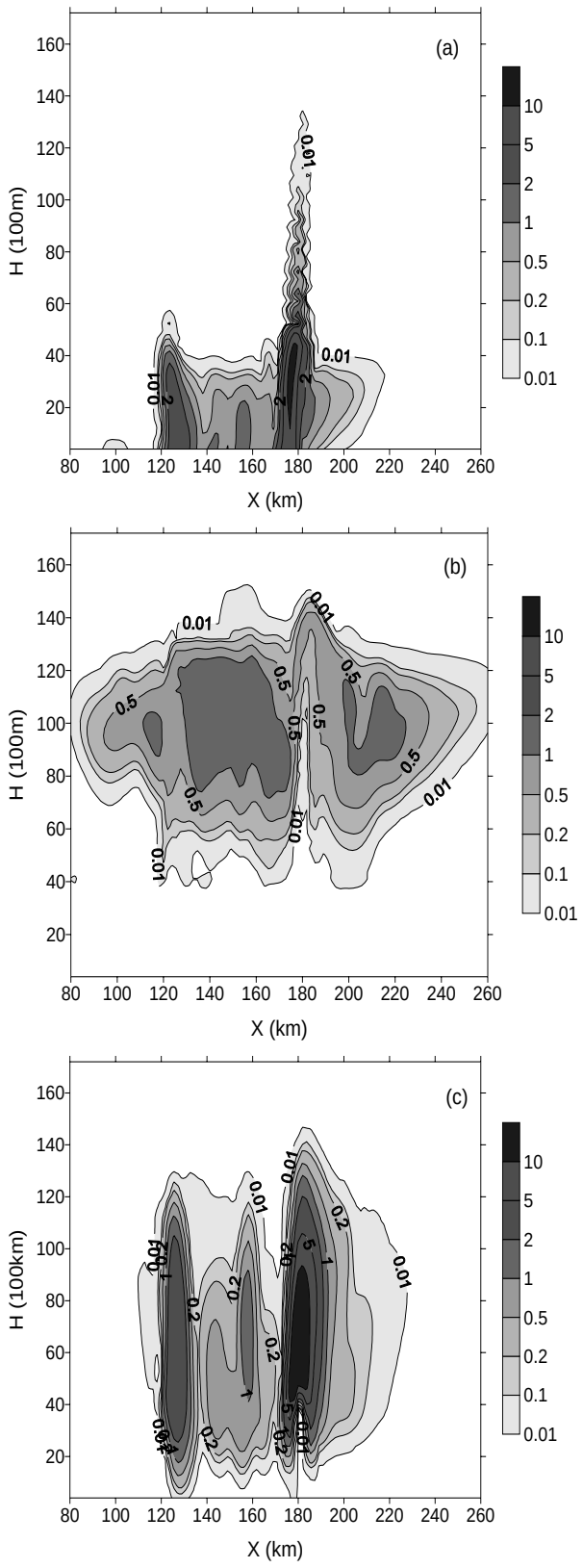

Fig. 6. Vertical cross sections of (a) q_r, (b) q_s, and (c) q_g at $y = 78$ km.

snow and graupel at $y = 78$ km. The large rain content (> 10 g m^{-3}) is located at the 4-km height and the supercooled water particles are carried to the 12-km height by strong updraft. The maximum snow content of 2 g m^{-3} is located at the 10-km height. In the updraft region, the snow content reaches its minimum. The graupel content begins to decrease below the level of 4 km and most of the grapuel is melted into rain at the 2-km height. Figure 7 shows the poloarimetric variables corresponding to Fig. 6. The high Z_H above 4 km is mainly contributed to by graupel, supercooled water and snow. Below that level, the rain and melting graupel cause high reflectivity. An obvious "bright-band" is observed at the 4-km height in Fig. 7a due to the melting of snow and graupel. The Z_{DR} of snow and graupel is near zero above 4 km and increases with the melting of graupel. It reaches 2.5 dB near the ground. The melting processes of graupel and snow produce more rain content and reduce the snow and graupel contents. Both of these processes increase Z_{DR}. The two high Z_{DR} regions are produced by raindrops. K_{DP} increases below the height of 4 km, which is mainly caused by raindrops.

The interesting vertical distribution of $|\rho_{HV}(0)|$ is produced by the algorithm. The $|\rho_{HV}(0)|$ of snow is about 0.97 above 7 km, but $|\rho_{HV}(0)|$ is reduced with height due to the graupel content increase between 7 and 4 km. The melting of snow and graupel cause a sharp reduction of $|\rho_{HV}(0)|$ between 4 and 2 km. Below the height of 2 km, most of the ice-phased particles are melted into rain, hence the high $|\rho_{HV}(0)|$. The vertical distribution of $|\rho_{HV}(0)|$ is consistent with the observation results (Schuur et al., 2003).

4. Conclusion and discussion

A polarimetric variable retrieval algorithm is developed and examined by using the ARPS output data. The effects of the melting process and temperature on the polarimetric variables are considered in the algorithm. An algorithm of $|\rho_{HV}(0)|$ for a mixture of a varied catalog of hydrometeors is introduced. The Z_H, Z_{DR}, and K_{DP} of rain are calculated quantitatively. But these polarimetric variables for snow and graupel, and ρ_{HV} for all hydrometeors, can only be evaluated qualitatively. The estimated polarimetric variables based on the ARPS model outputs are reasonable in that they are consistent with the microphysical processes in the atmosphere. The features of these variables near the 0°C level are reproduced successfully. The effects of the melting processes of hydrometeors on polarimetric variables are also reproduced by the algorithm.

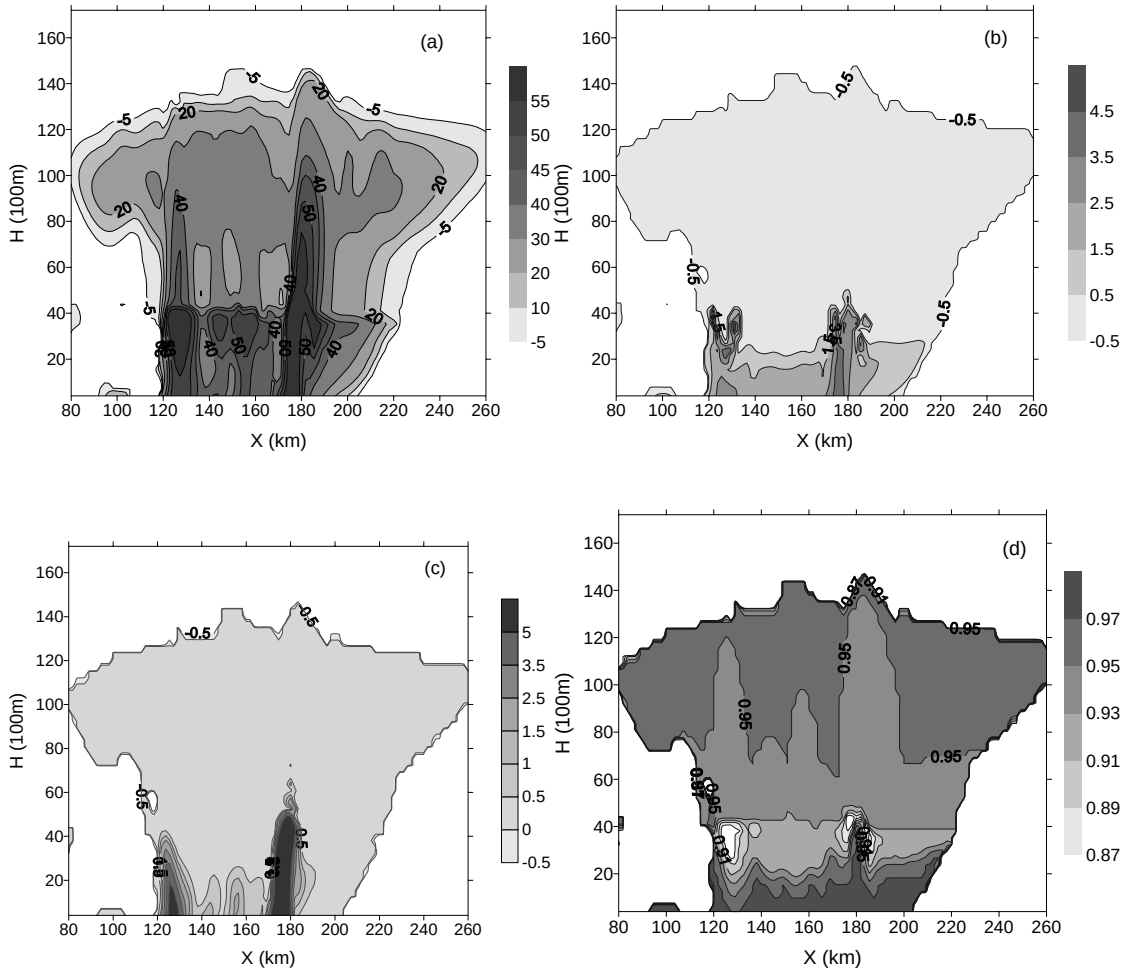

Fig. 7. Vertical crose sections of (a) reflectivity, (b) differential reflectivity, (c) specific phase shift, and (d) correlation coefficient at y=78 km.

It should be noted that the microphysics processes that occur under real weather conditions are more complicated than those described in the ARPS model. The drop size distribution in real precipitation is different from the assumptions of the Marshall and Palmer distribution used in the retrieval algorithm. In addition, the interactions between different types of hydrometeors are not considered in the algorithm. The retrieval results in the paper should be compared with dual linear polarization radar observations.

REFERENCES

Balakrishnan, N., and D. S. Zrnic, 1990: Use of polarization to characterize precipitation and discriminate large hail. *J. Atmos. Sci.*, **47**, 1525–1540.

Brandes, E. A., A. V. Ryzhkov, and D. S. Zrnic, 2001: An evaluation of radar rainfall estimates from specific differential phase. *J. Atmos. Oceanic Technol.*, **18**, 363–375.

Brunkow, D., V. N. Bringi, P. Kennedy, and S. Rutledge, 2000: A description of the CSU-CHILL national radar facility. *J. Atmos. Oceanic Technol.*, **17**, 1596–1608.

Dixon, M., and G. Wiener, 1993: TITAN: Thunderstorm Identification, Tracking, Analysis, and Nowcasting—A radar-based methodology. *J. Atmos. Oceanic Technol.*, **10**, 785–797.

Doviak, R., and D. S. Zrnic, 1993: *Doppler Radar and Weather Observation*. Academic Press, 209–279.

Doviak, R., V. N., Bringi, A. Ryzhkov, A. Zahrai, and D. Zrnic, 2000: Consideration for polarimetric upgrades to WSR-88D radar. *J. Atmos. Oceanic Technol.*, **17**, 257–278.

Gorgucci, E., V. Chandrasekar, V. N. Bringi, and G. Scarchilli, 2002: Estimation of raindrop size distribution parameters from polarimetric radar measurements. *J. Atmos. Sci.*, **59**, 2373–2384.

Hodur, R. M., 1997: The Naval Research Laboratory's Coupled Ocean/Atmosphere Mesoscale Prediction System (COAMPS). *Mon. Wea. Rev.*, **125**, 1414–1430.

Hubbert, J. V., V. N. Bringi, and L. D. Carey, 1998: CSU-CHILL polarimetric radar measurements from a severe hail storm in Eastern Colorado. *J. Appl. Meteor.*, **37**, 749–775.

Jameson, A. R, 1989: The interpretation and meteorological application of radar backscatter amplitude ratios at linear polarizations. *J. Atmos. Oceanic Technol.*, **6**, 908–919.

Klemp, J. B., and D. R. Durran, 1983: An upper boundary condition permitting internal gravity wave radiation in numerical mesoscale models. *Mon. Wea. Rev.*, **111**, 430–444.

Lin, Y. L., R. D. Farley, and H. D. Orville, 1983: Bulk parameterization of the snow field in a cloud model. *J. Appl. Meteor.*, **22**, 1065–1092.

Liu, H. P., and V. Chandrasekar, 2000: Classification of hydrometeors based on polarimetric radar measurements: Development of fuzzy logic and neuro-fuzzy systems and *in situ* verification. *J. Atmos. Oceanic Technol.*, **17**, 140–164.

Marshall, J. S., and W. Palmer, 1948: The distribution of raindrops with size. *J. Meteor.*, **5**, 165–166.

Nascimento, E. L., 2002: Dynamic Adjustment in an Idealized Numerically-Simulated Bow Echo. Ph. D dissertation, University of Oklahoma, 301pp.

Pierce, C. E., and P. J. Hardaker. 2000: GANDOLF: A system for generating automated nowcasts of convective precipitation. *Meteor. Appl.*, **7**, 341–360.

Qiu, C. J., and Q. Xu, 1992: A simple adjoint method of wind analysis for single-Doppler data. *J. Atmos. Oceanic Technol.*, **9**, 588–598.

Ryzhkov, A. V., and D. S. Zrnic, 1996: Assessment of rainfall measurement that uses specific differential phase. *J. Appl. Meteor.*, **35**, 2080–2090.

Ryzhkov, A. V., and D. S. Zrnic, 1998: Discrimination between Rain and Snow with a Polarimetric Radar. *J. Appl. Meteoro.*, **37**, 1228–1240.

Ryzhkov, A., and D. S. Zrnic, 2003: Discrimination between rain and snow with polarimetric NEXRAD radar. Preprints, *31st Conference on Radar Meteorology*, Seattle, WA, Amer. Meteor. Soc., 635–638.

Ryzhkov, A. V., D. S. Zrnic, and B. A. Grdon, 1998: Polarimetric method for ice water content determination. *J. Appl. Meteor.*, **37**, 125–134.

Sachidananda, M., and D. S. Zrnic, 1987: Rain rate estimates from differential polarization measurements. *J. Atmos. Oceanic Technol.*, **4**, 588–598.

Schuur, T., A. Ryzhkov, P. Heinselman, D. S. Zrnic, D. Burgess, and K. Scharfenberg, 2003: Observations and classification of echoes with polarimetric WSR-88D radar. Report of National Severe Storm Laboratory, Norman, OK, 46pp.

Seliga, T. A., V. N. Bringi, and H. H. Al-Khatib, 1981: A preliminary study of comparative measurements of rainfall rate using the differential reflectivity radar technique and a raingauge network. *J. Appl. Meteor.*, **20**, 1362–1368.

Smith, P. L. Jr., C. G. Myers, and H. D. Orville, 1975: Radar reflectivity factor calculations in numerical cloud models using bulk parameterization of precipitation. *J. Appl. Meteor.*, **14**, 1156–1165.

Straka, J. M., D. S. Zrnic, and A. V. Ryzhkov, 2000: Bulk hydrometeor classification and quantification using polarimetric radar data: Synthesis of relations. *J. Appl Meteor.*, **39**, 1341–1372.

Sun, J., and N. A. Crook, 1997: Dynamical and microphysical retrieval from Doppler radar observations using a cloud model and its adjoint. Part I: Model development and simulated data experiments. *J. Atmos. Sci.*, **54**, 1642–1661.

Vivekanandan, J., V. N. Bringi, M. Hagen, and P. Meischner, 1994: Polarimetric radar studies of atmospheric ice particles. *IEEE Trans. Geosci. Remote Sens.*, **32**, 1–10

Vivekanandan, J., S. M. Ellis, R. Oye, D. S. Zrnic, A. V. Ryzhkov, and J. Straka, 1999: Cloud microphysics retrieval using S-band dual-polarization radar measurements. *Bull. Amer. Meteor. Soc.*, **80**, 381–388.

Vivekanandan, J., R. Raghavan, and V. N. Bringi, 1993: Polarimetric radar modeling of mixtures of precipitation particles. *IEEE Trans. Geosci. Remote Sens.*, **31**, 1017–1030.

Wilson, J. W., and C. K. Mueller, 1993: Nowcasts of thunderstorm initiation and evolution. *Wea. Forecasting,* **8**, 113–131

Xue, M., K. K. Droegemeier, and V. Wong, 1995: The Advanced Regional Prediction System and real-time storm weather prediction. Preprints, *International Workshop on Limited-Area and Variable Resolution Models*, Beijing, China, WMO, 7pp.

Xu, Q., H. D. Gu, and C. J. Qiu, 2001: Simple adjoint retrievals of wet-microburst winds and gust-front winds from single-Doppler radar data. *J. Appl. Meteor.*, **40**, 1485–1499.

Zrnic, D. S., and A. V. Ryzhkov, 1998: Observations of insects and birds with a polarimetric radar. *IEEE Trans. Geosci. Remote Sens.*, **36**, 661–668.

Zrnic, D. S., N. Balakrishnan, C. L. Ziegler, V. N. Bringi, K. Aydin, and T. Matejka, 1993: Polarimetric signatures in the stratiform region of a mesoscale convective system. *J. Appl. Meteor.*, **32**, 678–693.